Cramer-Rao Lower Bound for Performance Analysis of Leak Detection

Alireza Keramat[1]; Mohamed S. Ghidaoui, M.ASCE[2]; Xun Wang[3]; and Moez Louati[4]

Abstract: Due to random noise in real measurements, leak detection (estimation of leak size and location) is subject to a degree of uncertainty. This paper provides a framework to investigate the lower bound of the variance of a leak's variable estimation and delineates the parameters upon which this lower bound depend. This is accomplished by applying the Cramer-Rao lower bound (CRLB) principle to the leak detection problem. For a given data set, CRLB gives the minimum mean square error of any unbiased estimator. The CRLB is evaluated using the Fisher information, which is evaluated from direct differentiation of the water-hammer characteristics equations. The results show that the CRLB of the leak-size estimate increases with time of closure and noise level but reduces with the duration of the measured signal. It is also shown that the CRLB is instrumental in the systematic design of efficient transient tests for leak detection. The error of leak-size estimates rises remarkably with setting distances between consecutive potential leaks of less than half the minimum wavelength of the probing signal. More conclusions are drawn on appropriate mesh-size for inverse transient analysis (ITA), maximum possible accuracy in successful localization, and its probability subject to the physical situation's parameters. **DOI: 10.1061/(ASCE)HY.1943-7900.0001603.**

Author keywords: Leak detection; Inverse transient analysis; Cramer-Rao lower bound; Water hammer; Noise; Method of characteristics; Performance limits; Direct differentiation method.

Introduction

Leakage in pipe systems is a serious and growing concern in water resources management. Therefore, leak detection techniques, especially those based on transient tests, are receiving great attention from scientists (Colombo et al. 2009). The purpose of transient-based defect detection methods (TBDDM) is to infer some unknown properties of a pipe system from measured pressure transient signals (Liggett and Chen 1994; Colombo et al. 2009). This is done through a procedure consisting of mathematical modeling, numerical simulation, use of an optimization tool (often), identification of model input parameters, and data collection from experimental tests. Each of these tasks is prone to some amount of error, which finally leads to uncertain results from the TBDDM. These errors mean that TBDDM results need to be interpreted using a statistical framework (Duan 2016; Sattar and El-Beltagy 2017). This approach for TBDDM is in its infancy, but is beginning to bear fruit (e.g., Vitkovsky et al. 2007; Lee et al. 2015; Wang and Ghidaoui 2018b; Zhao et al. 2018).

Measurement errors can be categorized into systematic error (deterministic error) and noise (random error or statistical uncertainty). Systematic error can be due to a miscalibration of measuring devices, which is deterministic in principle, or due to modeling assumptions and approximations. Noise, on the other hand, is described as random fluctuations around a mean value (e.g., uncertain mechanical motion of particles), which makes all measured data uncertain. The pressure spikes of noise do not contain any information about the system properties, but their partial resemblance to true reflections from leaks (i.e., pressure drops) causes the deterioration of the signal and results in either inaccurate estimation of leak parameters or even the wrong identification (e.g., identification of leaks that do not exist or missing leaks that do exist) (Ferrante et al. 2007, 2010, 2016).

Estimation theory provides a lower bound of the mean square error of the parameters being investigated as a function of measured signal characteristics (bandwidth, power, and time length). This lower bound is referred to as the Cramer-Rao lower bound (CRLB) and is quantified by the Fisher information matrix (Kay 1993). In the case of multiple unknown parameters to be estimated, the CRLB offers a lower bound for their covariance matrix (Kay 1993; Garthwaite et al. 2002; van Trees and Bell 2013).

CRLB has a number of practical applications. For example, it can be used to evaluate different estimators [i.e., different TBDDM approaches to see which one comes close or achieves the theoretical lower bound (Vaseghi 2008)]. In addition, the CRLB provides a framework for assessing how the various parameters that are under the control of the experimenter (e.g., characteristics of input signal and length of measured signal, among others) affect the estimation and how to choose the best strategy to minimize the minimum square error of the parameters being estimated (e.g., Diong et al. 2015; Bolliger et al. 2013; Zhao et al. 2014).

This paper introduces the CRLB approach to the TBDDM and formulates a fast, accurate, and efficient scheme for evaluating the CRLB from water-hammer characteristics equations. The effect of

[1]Research Associate, Dept. of Civil and Environmental Engineering, Hong Kong Univ. of Science and Technology, Clear Water Bay, Hong Kong, China; Assistant Professor, Dept. of Civil Engineering, Jundi-Shapur Univ. of Technology, Dezful, Iran (corresponding author). ORCID: https://orcid.org/0000-0002-6280-4931. Email: alireza.keramat@gmail.com

[2]Chinese Estates Professor of Engineering and Chair Professor, Dept. of Civil and Environmental Engineering, Hong Kong Univ. of Science and Technology, Clear Water Bay, Hong Kong, China. Email: ghidaoui@ust.hk

[3]Research Associate, Dept. of Civil and Environmental Engineering, Hong Kong Univ. of Science and Technology, Clear Water Bay, Hong Kong, China. Email: xunwang00@gmail.com

[4]Research Assistant Professor, Dept. of Civil and Environmental Engineering, Hong Kong Univ. of Science and Technology, Clear Water Bay, Hong Kong, China. ORCID: https://orcid.org/0000-0003-4661-7164. Email: mlouati@connect.ust.hk

Note. This manuscript was submitted on June 25, 2018; approved on November 27, 2018; published online on March 29, 2019. Discussion period open until August 29, 2019; separate discussions must be submitted for individual papers. This paper is part of the ***Journal of Hydraulic Engineering***, © ASCE, ISSN 0733-9429.

valve closure time, duration of measurement, and signal power on the accuracy of localization and leak-size estimates is investigated. In addition, the computed CRLB values of the leak variables are used to estimate minimum possible standard deviation of leak areas.

The paper is structured as follows. In the next section, the role of CRLB in leak detection is elucidated. Then, the numerical scheme to compute CRLB is formulated and validated, and its computational properties are discussed. Numerical examples and computations of performance limits for a typical reservoir-pipe-valve system are then discussed. Two applications of the proposed CRLB computations (design of experiments and probability of successful localization of leaks) are discussed.

CRLB and Its Role in Transient-Based Defect Detection

In real experiments, measurements are always contaminated by random noise. As a result, detecting defects (leaks in this paper) requires a statistical framework. It is thus natural to ask what, given an experimental setup and the distribution of random noise, is the optimal leakage detection result? That is, what is the minimum possible square error of leakage localization? This is precisely the role of CRLB theory (Kay 1993). In particular, CRLB provides the theoretical lower bound of the mean square error of parameter estimation. It is important to stress that the mean square error of maximum likelihood estimation (MLE) tends to the CRLB as the sample size tends to infinity (Garthwaite et al. 2002).

A reservoir-pipe-reservoir system is considered where the fluid is assumed inviscid. To elucidate the CRLB and its important role in transient-based defect detection, a leakage problem for which the CRLB can be derived analytically is considered (Wang et al. 2019)

$$\mathrm{CRLB}(x_L) = \frac{\sigma^2}{2SA_e^2\|G'(x_L)\|^2} \tag{1}$$

$$\text{with } \|G'(x_L)\|^2 = \sum_{j=1}^{J} \frac{Z^4 g q^2(x_U)}{2H_L^0} \sin^2\left(\frac{\omega_j}{a}(x_m - 2x_L)\right) \tag{2}$$

where S = sample size (number of times the experiment is repeated); x_L = leak location; A_e = effective leak area; σ^2 = noise variance; $Z = a/gA$ = pipe impedance; a = wave speed, g = gravity; A = cross-sectional area; $\omega_j = j$th selected angular frequency for leakage detection ($j = 1, \ldots, J$); $q(x_U)$ = transient flow rate at the upstream; H_L^0 = steady-state pressure head at the leak; and x_m = measurement position. Therefore, the minimum variance of the leak location estimate is analytically given by combination of Eqs. (1) and (2) as follows:

$$\mathrm{CRLB}(x_L) = \mathrm{var}(\hat{x}_L) = \frac{H_L^0\sigma^2}{SA_eZ^4gq^2(x_U)\sum_{j=1}^{J}\sin^2\left(\frac{\omega_j}{a}(x_m - 2x_L)\right)} \tag{3}$$

If all the parameters in the right-hand side are known, then the CRLB provides the minimum possible variance that any leakage detection scheme can achieve. This lower limit provides a quantitative measure for comparing different defect detection schemes (Wang et al. 2019). Furthermore, the right-hand side of Eq. (3) provides analysts with a scientific way to assess and design experiments so as to minimize the variance of the parameter being identified. For example, it is clear that to lower the minimum variance of leak estimate, it is better to measure during peak demand (i.e., when H_L^0 is small). This is consistent with the finding of Ferrante et al. (2014).

In addition, the CRLB shows that the larger the value of J (number of measured frequencies), the smaller the variance of the leak estimate. This dependence on frequency provides a theoretical support for the intuitive result that sharper transients (wider frequency bandwidth) result in more reliable (accurate) defect detection and agrees with the results found by Lee et al. (2013, 2015), Zhao et al. (2018), Louati et al. (2017), and Wang and Ghidaoui (2018b).

Moreover, the CRLB shows the relationship between sample size, S, and variance of leak localization. Furthermore, the CRLB shows explicitly how a larger leak size A_e and a smaller noise level σ^2 are beneficial for defect detection. For example, reducing the noise by half (which can be performed by repeated transient tests or larger S) reduced the variance of localization by a factor of 4. Taking derivatives of the CRLB with respect to the various parameters informs the analyst of the marginal gain in identification accuracy. For example, the decreasing rate (derivative) of the CRLB with respect to S provides the analyst with an increased level of confidence in localizing the leak by adding one more measurement.

The preceding discussion was given for the ideal case (e.g., no friction, linear leak law, and sudden valve closure). More realistic test cases where these assumptions are relaxed (Ferreira et al. 2018) cannot be analyzed analytically. Therefore, in what follows, the method of characteristics is used to investigate the CRLB for more realistic test cases.

Numerical Formulation of CRLB

The simple example in the previous section assumes one leak; thus, the uncertainty of both leak location and size is estimated. Wang and Ghidaoui (2018a) developed a linearized frequency-domain model and derived corresponding CRLB equations of leak size and location for any leak. However, for the time-domain water-hammer solution where several parameters may be incorporated in the model, an analytical solution for the CRLB cannot be derived, and a numerical approach is needed. Computational approaches allow for the application of a versatile transient solver that includes advanced models of viscoelasticity, turbulence, fluid–structure interaction, and non-Newtonian fluids, among others, with various types of boundary conditions (Covas et al. 2005; Ahmadi and Keramat 2010; Keramat and Tijsseling 2012; Keramat et al. 2012, 2013; Meniconi et al. 2014; Majd et al. 2016; Meniconi et al. 2017; Ferreira et al. 2018). In this view, any arbitrary valve type and consequently valve maneuver with any nonlinear closure pattern or pipe system equipment such as pumps or pressure suppression devices can be adopted in such numerical formulation. The majority of time-domain leak estimation models assume many equidistant leaks on the pipeline because they usually adopt method of characteristics (MOC) as the solver of the forward problem (Liggett and Chen 1994; Vítkovský et al. 2000; Brunone and Ferrante 2001; Kapelan et al. 2003; Covas et al. 2005; Jung and Karney 2008; Haghighi and Ramos 2012). In this view, this section derives a numerical procedure for evaluating the CRLB in a model with many equidistant leaks.

Before embarking on the validation section and the CRLB usage for realistic cases, the framework of numerical computation of CRLB is detailed. First, the fundamental equations and concepts are defined and then, the time-domain based numerical scheme for evaluating CRLB is described.

Numerical Computation of CRLB

One of the simplest CRLB formulations of unbiased estimators is numerically computed based on the Hessian of the likelihood function of leak estimates. If the elements of the measurement vector

$\mathbf{h_m}$ are independent and identically distributed, then the covariance matrix of measurements reduces to $\text{cov}(\mathbf{h_m}) = \sigma^2 \mathbf{I}_M$, in which σ^2 is the variance of random noise and $\mathbf{I}_M$ is the M-dimensional identity matrix. Therefore, the log-likelihood function becomes (Press et al. 1992; Oppenheim et al. 1983)

$$\ln \text{L}(\mathbf{A_e}; \mathbf{h_m}) = -\frac{M}{2}\ln(2\pi) - M\ln\sigma - \frac{1}{2\sigma^2}\|(\mathbf{h_m} - \mathbf{h})\|^2 \quad (4)$$

where $\mathbf{h}$ denotes the expectation of $\mathbf{h_m}$ and may be found by MOC solution. The CRLB then states that the covariance matrix of the unbiased leak-area estimators $\mathbf{A_e}$ satisfies

$$\text{cov}(\hat{\mathbf{A}}_\mathbf{e}) = \mathbb{E}\left[(\hat{\mathbf{A}}_\mathbf{e} - \mathbf{A_e})(\hat{\mathbf{A}}_\mathbf{e} - \mathbf{A_e})^{\text{T}}\right] \geq \mathbf{I}(\mathbf{A_e})^{-1} \quad (5)$$

where $\mathbf{I}(\mathbf{A_e})$ is the Fisher information matrix, whose element is

$$I_{i,j} = \mathbb{E}\left[\frac{\partial}{\partial A_{ei}}\ln \text{L}(\mathbf{A_e}; \mathbf{h_m})\frac{\partial}{\partial A_{ej}}\ln \text{L}(\mathbf{A_e}; \mathbf{h_m})\right] = -\mathbb{E}\left[\frac{\partial^2}{\partial A_{ei}\partial A_{ej}}\ln \text{L}(\mathbf{A_e}; \mathbf{h_m})\right], i, j = 1, 2, \ldots, N_L \quad (6)$$

Considering Eqs. (4) and (6), the second derivative of the last term of Eq. (6) is (Appendix I)

$$\frac{\partial^2}{\partial A_{ei}\partial A_{ej}}\ln \text{L}(\mathbf{A_e}; \mathbf{h_m}) = \frac{1}{\sigma^2}\left[\frac{\partial^2 \mathbf{h}^{\text{T}}}{\partial A_{ei}\partial A_{ej}}(\mathbf{h_m} - \mathbf{h}) - \frac{\partial \mathbf{h}^{\text{T}}}{\partial A_{ei}}\frac{\partial \mathbf{h}}{\partial A_{ej}}\right] \quad (7)$$

Thus, the CRLB corresponding to each element of the leak-areas covariance matrix reads

$$\Sigma_{\hat{\mathbf{A}}_\mathbf{e}} = \text{cov}(\hat{\mathbf{A}}_\mathbf{e}) \geq \mathbf{I}(\mathbf{A_e})^{-1}, \quad I_{i,j} = -\mathbb{E}\left[\frac{\partial^2}{\partial A_{ei}\partial A_{ej}}\ln \text{L}(\mathbf{A_e}; \mathbf{h_m})\right] = \frac{1}{\sigma^2}\frac{\partial \mathbf{h}^{\text{T}}}{\partial A_{ei}}\frac{\partial \mathbf{h}}{\partial A_{ej}} \quad (8)$$

Each element of the Fisher information matrix ($I_{i,j}$) is found by the scalar product of two vectors. The vector $\partial\mathbf{h}/\partial A_{ei}$ ($\partial\mathbf{h}/\partial A_{ej}$) means the derivative of the computed head vector at the measurement location with respect to the effective area of ith (jth) leak candidate. The numerical algorithms to compute the elements of these vectors ($\partial h_n/\partial A_{ei}$, $n = 1, 2, \ldots, M$) are addressed in the next section. The computed head is obviously a function of model inputs including time closure and closure pattern of valve, time-length of analysis, pipeline and flow properties, and leak variables. As seen in the last expression of Eq. (8), the lower bound of the covariance matrix of estimated parameters is independent of a specific measurement vector and is only a function of the statistical properties of the random vector $\mathbf{h_m}$ (i.e., computed head, its variance, and distribution).

A sensible global measure of performance of an estimator $\hat{\mathbf{A}}_\mathbf{e}$ is defined by the root-mean square error (RMSE)

$$\text{RMSE}(\mathbf{A_e}) = \left(\frac{1}{N_L}\mathbb{E}[(\hat{\mathbf{A}}_\mathbf{e} - \mathbf{A_e})^{\text{T}}(\hat{\mathbf{A}}_\mathbf{e} - \mathbf{A_e})]\right)^{\frac{1}{2}} \quad (9)$$

which indicates the root-mean square error performance over the entire N_L leak candidates. The corresponding Cramer-Rao (CR) inequality can be introduced using the trace of computed matrix $\mathbf{I}(\mathbf{A_e})^{-1}$ in Eq. (8) as follows (Vitkovsky et al. 2003; Nehorai and Hawkes 2000; Robinson and Milanfar 2006):

$$\text{RMSE}(\mathbf{A_e}) \geq \xi(\mathbf{A_e}), \quad \text{with} \quad \xi(\mathbf{A_e}) = \left(\frac{1}{N_L}\text{trace}(\mathbf{I}^{-1})\right)^{\frac{1}{2}} \quad (10)$$

This measure of performance has units of leak area and represents the minimum average error of size estimation.

Numerical Computation of Sensitivities

The elements of the vector $\partial\mathbf{h}/\partial A_{ei}$ in Eq. (8) are $\partial h_n/\partial A_{ei}$, $n = 1, 2, \ldots, M$, where n indicates the time step. They represent the sensitivity of the computed pressure heads at the nth time step with respect to the ith model parameter A_{ei}, $i = 1, 2, \ldots, N_L$. This derivative can be approximated by finite difference for all leak-size parameters. However, this numerical calculation becomes cumbersome when the number of parameters are high because each numerical derivative computation requires running the solver. An alternative approach to calculate gradients is the adjoint method (Liggett and Chen 1994). Using this method, the forward and adjoint solvers are called once, and hence the number of computations is remarkably reduced. However, the derivation of the continuous adjoint equations is complicated, especially when unsteady friction, viscoelasticity, or nonlinear boundary conditions are taken into account.

In this research, the direct differentiation method (DDM) is developed, which is an accurate and computationally efficient alternative method for computing the response sensitivities. The proposed DDM, explained in Appendix II in detail, is based on the exact differentiation (consistent calculation of state variables) of the compatibility equations with respect to the model parameters. This approach was previously used by Nash and Karney (1999) for the calibration of friction coefficient in the inverse transient analysis (ITA), and it is also widely used in structural mechanics when time-domain solutions are adopted (Kleiber et al. 1997; Conte et al. 2003).

Validation and Convergence of CRLB Computation

This section verifies the proposed numerical scheme to evaluate CRLB. The numerical computations are conducted in a typical reservoir-pipe-valve system with one leak in the middle. The system specifications are wave speed $a = 1{,}000$ ms^{-1}, pipe length $L = 1{,}000$ m, inner diameter of pipe = 0.2 m, upstream reservoir head $h_R = 26$ m, outflow velocity from reservoir (before the leak) = 0.2 ms^{-1}, friction factor of pipe flow $f = 0$, effective leak area $A_e = 20$ mm^2, valve maneuver time (linear) $T_c = 0.04$, signal to noise ratio (SNR) = 10 dB, and signal length (total time of measurement) $T_T = 2T$, where $T = 4$ s is the fundamental water-hammer period.

The mesh size of MOC is refined and the number of leak candidates is taken as constant. Fig. 1 shows the convergence of CRLB results indicated by error bars when the number of leak candidates is fixed to $N_L = 19$ so that distance between potential leaks is $d = 50$ m whereas the grid size (Δx) decreases. As seen, despite making use of finer mesh than 50 m, the computed standard deviations still arrive at relatively the same quantity, which implies that the CRLB computations soon converge to a quantity. This in turn validates the proposed numerical application of CRLB. The negative error bars in Fig. 1 are due to the unbiased estimation method used to compute CRLB. Unbiasedness means that expectation of an estimator is equal to its actual value. Because the expected values of the estimated leak sizes at nonleaky nodes are zero, negative leak sizes are possible, which in fact compensates for positive sizes to keep the mean equal to zero (if estimation is repeated several times).

The trend of convergence with the mesh size can better be studied by the average of standard deviations defined by Eq. (10). Fig. 2 depicts the convergence of the measure (trace of the inversion of the Fisher information matrix) defined by Eq. (10), which is a key parameter to quantify the performance of the leak-size estimation.

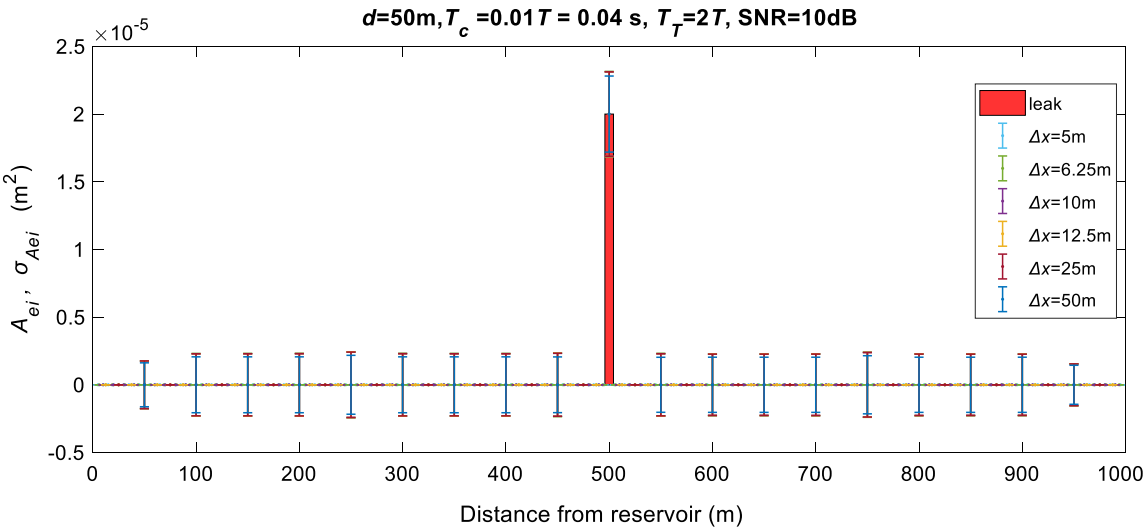

Fig. 1. Convergence of computed standard deviations at leak candidates for different mesh grids Δx and fixed distance between leaks $d = 50$ m. Solid bar indicates actual leak size and location.

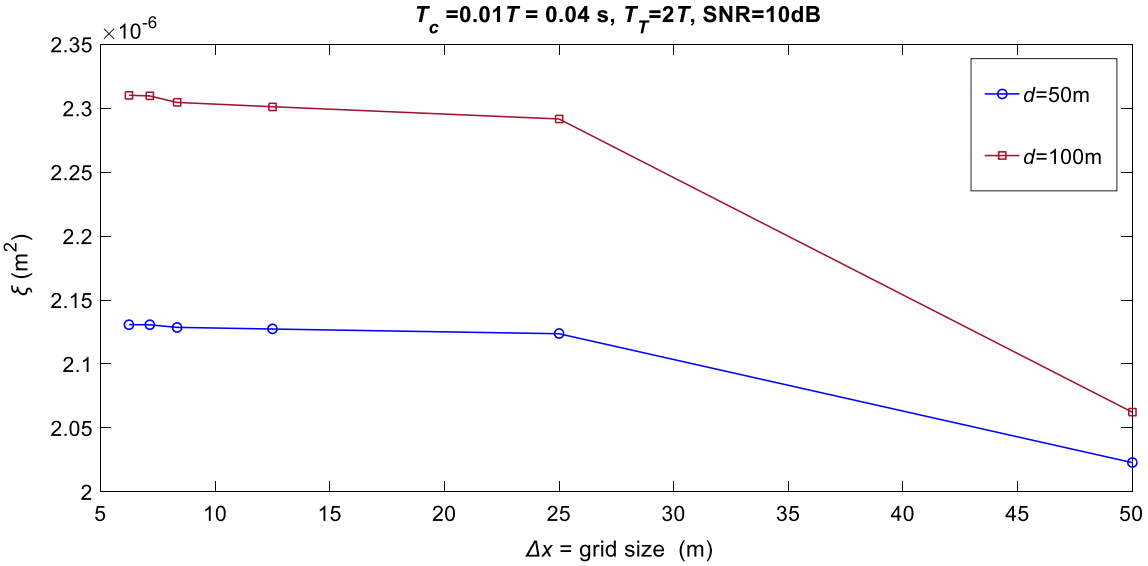

Fig. 2. Convergence of the performance bound ξ defined in Eq. (10) versus gird size (Δx) for two different spacing of leak candidates: $d = 50$ m and $d = 100$ m.

The figure represents the convergence of ξ for two different numbers of potential leaks: $N_L = 19$ and $N_L = 9$, which correspond to leak distances of 50 and 100 m, respectively. In both cases, the convergence occurs for mesh sizes around $0.5\ a \cdot T_c = 20$ m, which can be adopted as an appropriate mesh size for the proposed numerical computation.

Spatial Resolution of Leak Estimates

This section investigates the effect of space resolution (i.e., spacing between potential leaks = d) on the CRLB results. Intuitively, reducing the distance between computational leaky nodes in MOC codes gives better accuracy. However, this section indicates that this is not always true in leak detection. In fact, the accuracy depends on the amount of information collected during transients.

According to the test case specified in the previous section, Figs. 3(a–f) give the standard deviation (CRLB analysis results) at leak candidates for six cases of space resolution including $d =$ 166.67, 100, 50, 25, 16.67, and 12.5 m, respectively, where they all come together in Fig. 3(g). Figs. 3(a–c) show that for $d \geq 50$ m, the minimum standard deviations do not change, and thus they are independent of the space resolution for this case. However, when $d < 50$ m [Figs. 3(d–f)], the precision reduces as the resolution increases. To explain this, the minimum wavelength of the probing signal, which is approximated by the length of the wavefront evaluated by $a \cdot T_c$, is equal to 40 m in all numerical simulations of this figure. Therefore, in the cases in Figs. 3(a–c) $d > a \cdot T_c$, whereas the cases in Figs. 3(d–f) correspond to $d < a \cdot T_c$. To conceive how the accuracy is related to the waveform, Fig. 4 depicts a schematic of a typical wavefront for two test cases. Fig. 4 illustrates that when the wavefront is larger than space resolution, neighboring leak nodes can interact with each other during the propagation of the wavefront. Such interaction allows for larger leak sizes (which means higher leak-size deviations) to reconstruct the indicated wavefront (and the

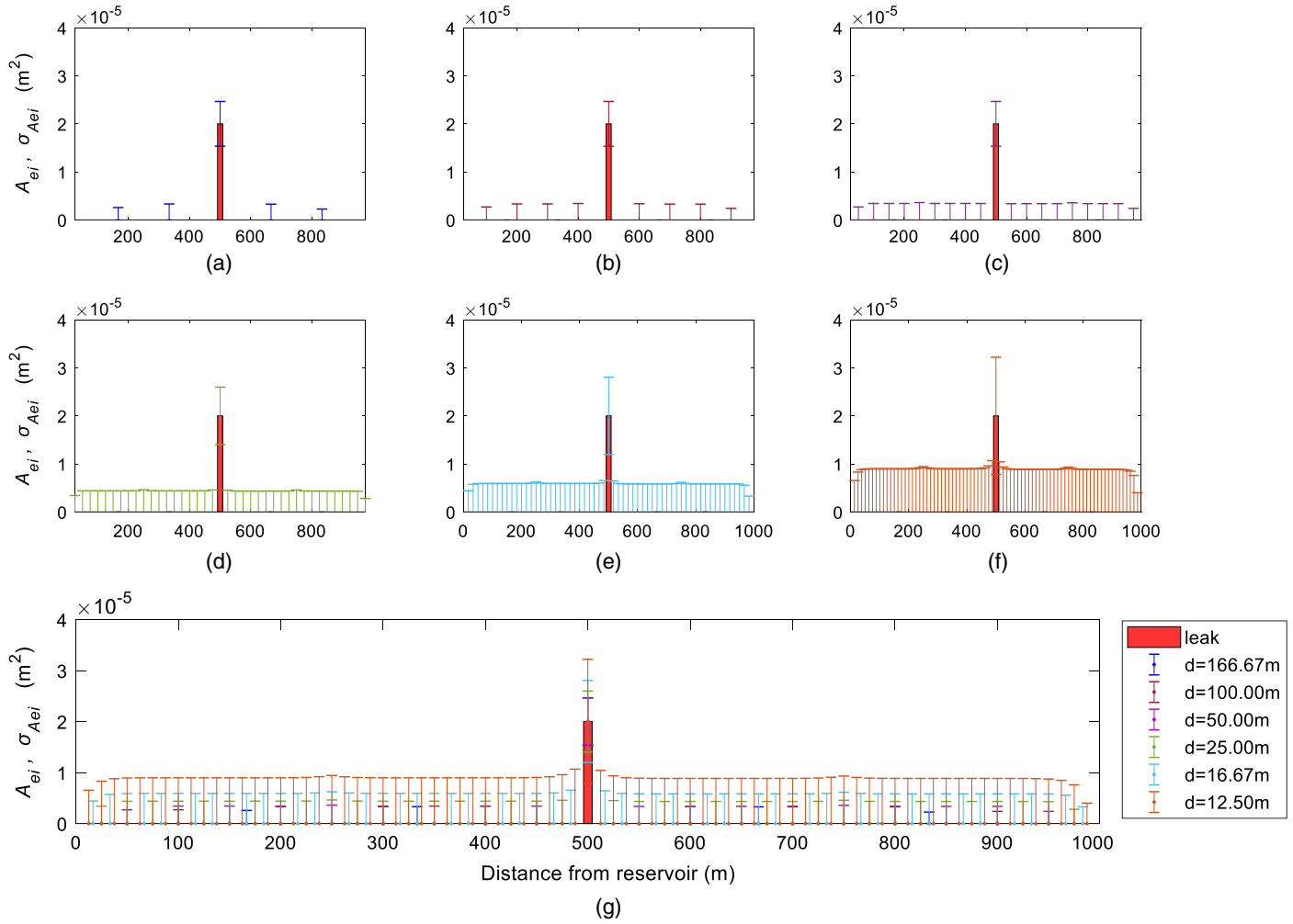

Fig. 3. Standard deviations at each leak candidate for different leak distances: (a) $d = 166.67$ m; (b) $d = 100$ m; (c) $d = 50$ m; (d) $d = 25$ m; (e) $d = 16.67$ m; (f) $d = 12.5$ m. $T_c = 0.01T = 0.04$ s and $a \cdot T_c = 40$ m; and (g) all the six leak distances. Solid bars indicate the actual leak size and location.

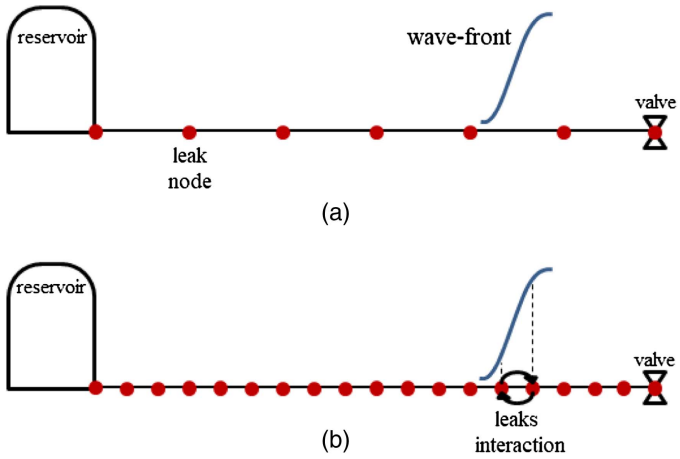

Fig. 4. Space resolutions versus leaks interaction.

whole collected signal) and hence reduces the accuracy of leak detection. Another justification for the leak interactions is provided in terms of correlation between leak-size estimates in Appendix III.

The trend of precision variations with space resolution can be further elucidated with the performance bound defined in Eq. (10). As shown in Fig. 5, when the leak distance is larger than minimum wavelength $\lambda = a \cdot T_c$, the average of standard deviations evaluated by Eq. (10) stays almost at the same level. As the leak distance decreases from λ to $\lambda/2$, CRLB slightly increases, but after $\lambda/2$, it drastically rises. This means that when $d < \lambda/2$, leaks cannot be efficiently identified. Consequently, the spacing of potential leaks is advised to be equal to half of minimum wavelength. This result is in agreement with the Nyquist-Shannon theory (Shannon 1949) and recent studies of transient-based leak detection by Wang and Ghidaoui (2018b) that two leaks with a distance lower than half of the minimum wavelength cannot be identified.

Analysis of the CRLB Model and Applications in Leak Detection

The purpose of this section is to illustrate the effects of noise and signal bandwidth and demonstrate how the time of valve closure, signal strength (or SNR), and time length of measured data can help provide more information about a leak. In particular, this section shows that CR inequalities [Eq. (8)] can quantify the accuracy of leak detection in terms of mean square error of size estimations. The use of CRLB in designing transient experiments is also discussed. Subsequently, it is deduced that the lower-bound errors of

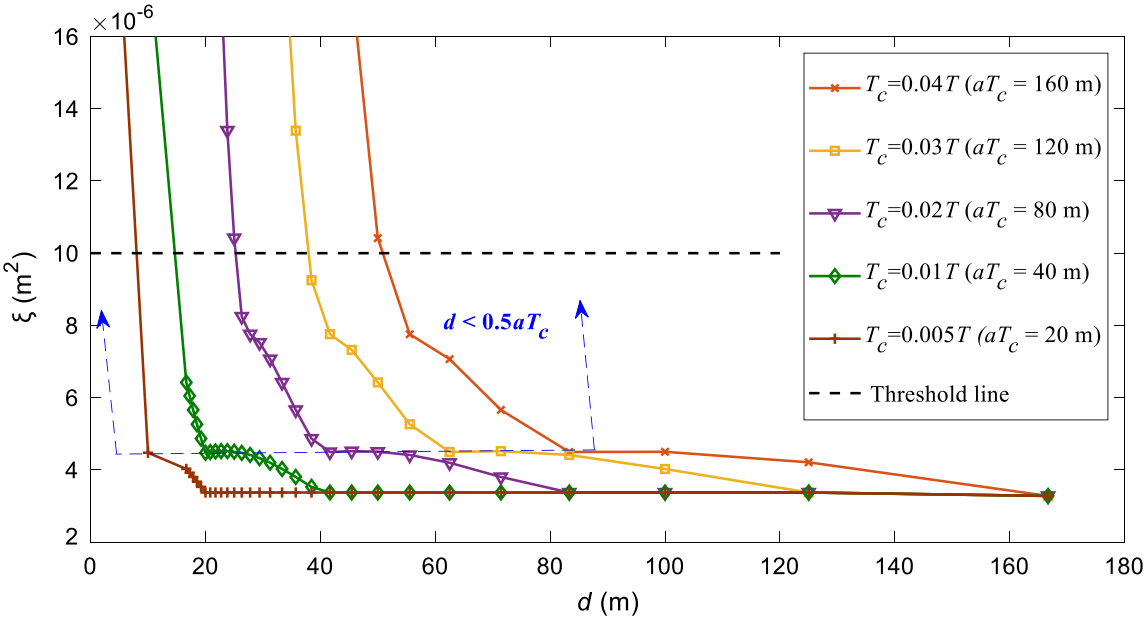

Fig. 5. Performance bound of vector $\hat{\mathbf{A}}_\mathbf{e}$ evaluated according to Eq. (10), ξ, versus distance between two consecutive leak candidates (resolution) d for different times of valve maneuver with $x_L = 500$ m, $A_e = 20$ mm^2, SNR = 10 dB, and $T_T = 2T$.

potential leak sizes provide considerable insight into spatial resolution and probability of successful leak localization.

The numerical computations are conducted in a typical reservoir-pipe-valve system with one or two leaks and the detailed properties specified earlier in the "Validation and Convergence of CRLB Computation" section.

Effect of Transient Test Parameters on CRLB

The main transient test parameters are valve maneuver time (i.e., frequency bandwidth), signal length measured and processed, and SNR (i.e., power of the generated transient amplitude versus noise level). The effect of these parameters on CRLB is investigated in this section through different numerical test cases. Fig. 6 gives the minimum standard deviations of leak sizes at each leak candidate. The distance between the possible leak positions is fixed to $d = 50$ m, which defines the spatial resolution of leak location. Figs. 6(a and b) illustrate the effect of frequency bandwidth where SNR and T_T are fixed to 10 dB and $2T$, respectively, while T_c is altered from $0.01T$ to $0.1T$. Figs. 6(a and b) show that the increase in time closure (linear pattern), which is equivalent to reduction in frequency bandwidth, significantly declines the accuracy of leak-size estimation. This raises the failure possibility of localization exercise. A comparison of standard deviations in Figs. 6(b and c) delineates the effect of signal length increase from $T_T = 2T$ to $T_T = 5T$, thus demonstrating the accuracy enhancement with the increase in sample size. Finally, Figs. 6(c and d) illustrate the effect of SNR when it reduces from 10 to 5 dB. The comparison between these two figures reveals how the precision declines as SNR reduces.

Fig. 6(c) indicates that a superresolution localization of leaks can be expected. The term superresolution refers to the ability to recover the information beyond the Shannon-Nyquist limit (Puschmann and Kneer 2005; Greenspan 2008; McCutchen 1967). In the current work, this means identification of leaks located at distance apart lower than half minimum wavelength (i.e., $d < \lambda/2$, where $d = 50$ m is potential leak spacing and $\lambda/2 = 0.5a \cdot T_c = 200$ m represents half the minimum wavelength). Similar descriptions of the superresolution can be found in astronomy (Puschmann and Kneer 2005), medical imaging (Greenspan 2008), and microscopy (McCutchen 1967).

Fig. 7 gives the case where two leaks are located 50 m (solid bars) apart and shows clearly the conclusions drawn regarding Fig. 6. As seen in Figs. 7(b–d), there is no hope of successful localization within the 50-m resolution, although from the results, one can conclude that Case C provides better performance than Cases B or D. If a 50-m accuracy is of interest, higher signal bandwidth (than 2.5 Hz), measurement size, or signal power is required.

Experiment Design

This section explains the role of CRLB in order to design the most efficient transient test for leak detection. Considering that CRLB estimates the maximum attainable accuracy for given set of transient parameters (e.g., frequency bandwidth or time closure, signal length, and SNR), if one targets a specific resolution for leak detection, CRLB is able to provide the appropriate parameters to achieve such resolution. For example, if a water authority targets leak localization down to a minimum size of $A_{e,\text{target}}$, then CRLB analysis can be employed to estimate the minimum frequency bandwidth, signal length, and SNR to achieve the desired target for leak-size detection. To do so, the CR bound of the mean square error of size estimates defined in Eq. (10) is exploited. This performance bound represents the ideal average standard deviation for size estimation. The measure ξ can be used to compare the efficiency of different transient experiments by allocating a performance quantity to each experiment. To simplify making comparisons, a relative CR bound that indicates the ratio of ξ of one experiment to that of a reference one is incorporated. This ratio intuitively represents the performance limit of a transient experiment with respect to the reference one. This is illustrated through an example in the rest of this section.

Herein, all comparisons are made with respect to the reference experiment whose performance bound is $\xi(T_c = 0.01T, T_T = 2T, \text{SNR} = 10 \text{ dB}, d = 50 \text{ m}) = \xi_{\text{ref}} = 2$ mm^2, which corresponds to that of Fig. 6(a) discussed previously. Recall that in Fig. 6(a), the minimum standard deviation of size detection on average is about $\xi_{\text{ref}} = \bar{\sigma}_{A_e} = 2$ mm^2 and leaks smaller than 2 mm^2 cannot be

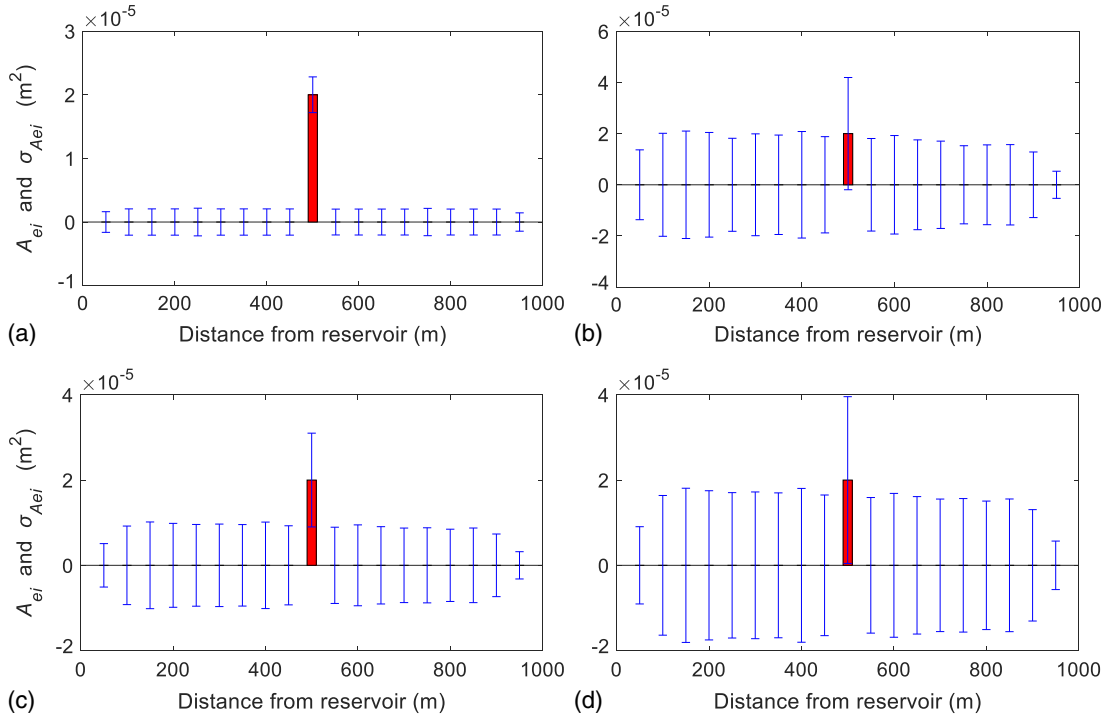

Fig. 6. Computed standard deviations at each leak candidate for different time closures, measurement size, and SNR: (a) SNR = 10 dB, $d = 50$ m, $T_T = 2T$, and $T_c = 0.01T$; (b) SNR = 10 dB, $d = 50$ m, $T_T = 2T$, and $T_c = 0.1T$; (c) SNR = 10 dB, $d = 50$ m, $T_T = 5T$, and $T_c = 0.1T$; and (d) SNR = 5 dB, $d = 50$ m, $T_T = 5T$, and $T_c = 0.1T$. Solid bars indicate actual leak size and location.

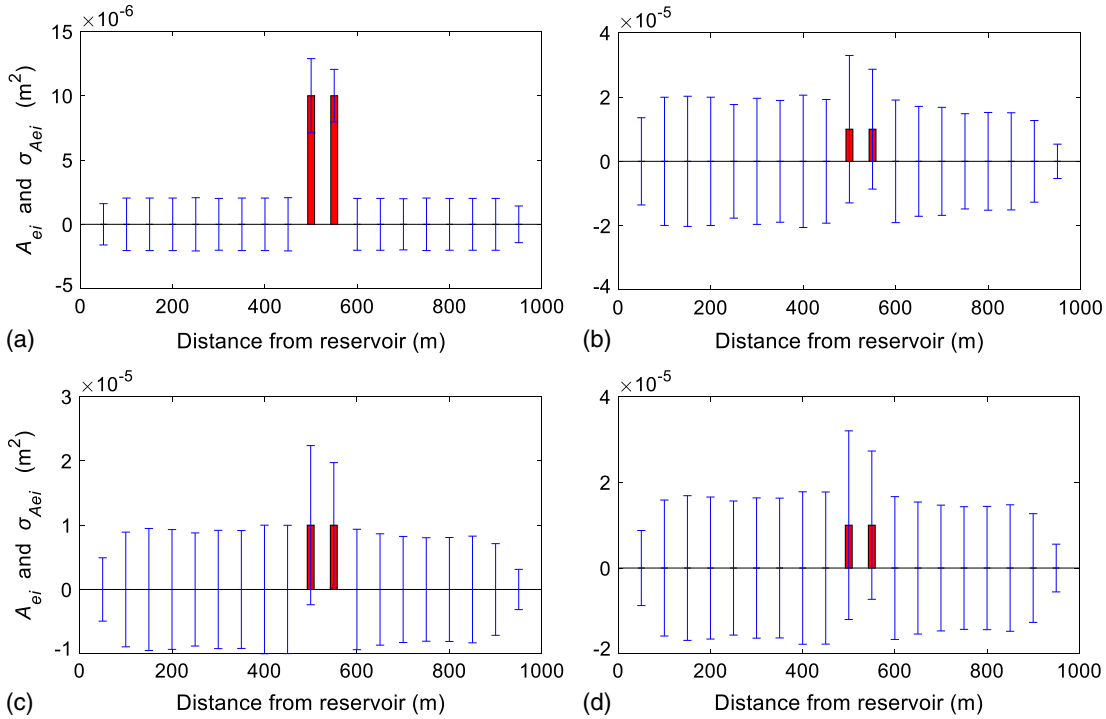

Fig. 7. Computed standard deviations at each leak candidate for different time closures, measurement size, and SNR: (a) SNR = 10 dB, $d = 50$ m, $T_T = 2T$, and $T_c = 0.01T$; (b) SNR = 10 dB, $d = 50$ m, $T_T = 2T$, and $T_c = 0.1T$; (c) SNR = 10 dB, $d = 50$ m, $T_T = 5T$, and $T_c = 0.1T$; and (d) SNR = 5 dB, $d = 50$ m, $T_T = 5T$, and $T_c = 0.1T$. Solid bars indicate actual leak size and location.

identified within the 50-m resolution. The ratio between the target size estimation and the aforementioned reference limit ξ_{ref} (detectable leak size) from CRLB is hereafter referred to as the relative CR bound and is indicated by ξ_r. Indeed, it defines the deviation bound of that experiment with respect to the reference one. As an example, for a target standard deviation $\xi_{\text{target}} = \bar{\sigma}_{A_e} = 4$ mm^2, the relative CR bound is $\xi_r = \xi_{\text{target}}/\xi_{\text{ref}} = 2$. The corresponding design curves for this example are further illustrated via some figures.

J. Hydraul. Eng., 2019, 145(6): 04019018

Figs. 8–10 give the variation of relative CR bound (ξ_r) with dimensionless time closure (i.e., frequency bandwidth), dimensionless signal length, and SNR, respectively. The relative bound $\xi_r = 2$ is indicated by arrows in these figures. Fig. 8 gives the variation of ξ_r with T_c/T for given $T_T = 2T$ and SNR = 10 dB, where T_c is the time closure (with linear maneuver) and T_T is the measurement length. The size estimation uncertainty (ξ_r) rises as the time closure increases, especially when T_c is higher than $0.5T$ (i.e., $T_c > 2L/a$). For the indicated target $\xi_r = 2$, CRLB shows that $T_c/T = 0.44$ is acceptable for the transient experiment.

Fig. 9 gives the variation of ξ_r with T_T for given $T_c = 0.01T$ and SNR = 10 dB. The figure displays that for a signal length larger

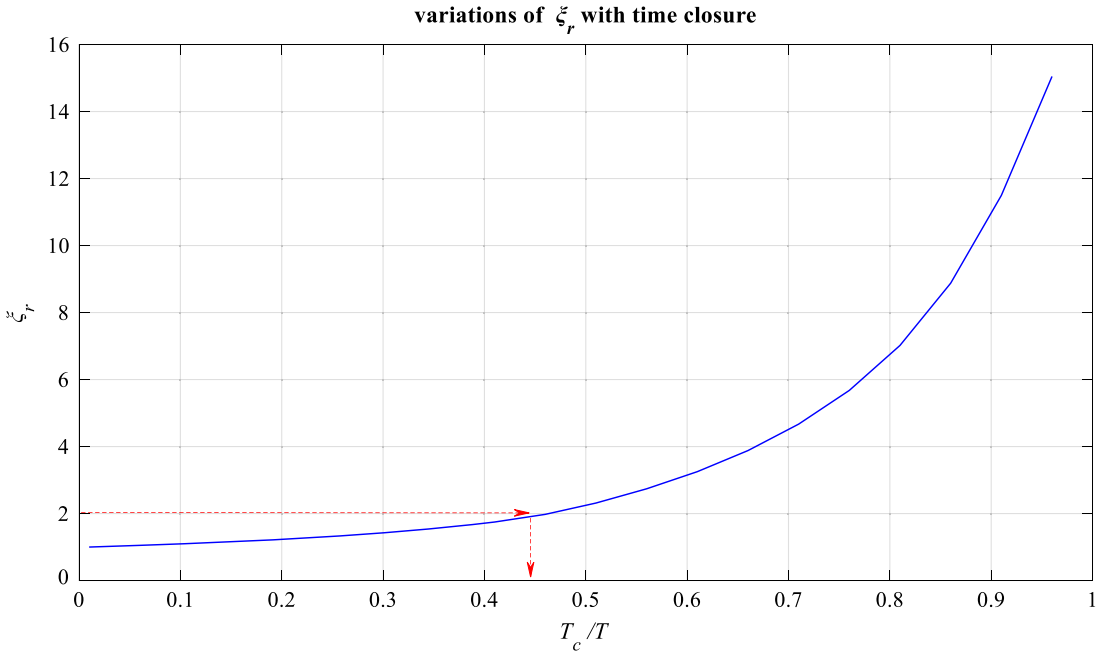

Fig. 8. Relative CR bound [Eq. (10) defines ξ] as a function of dimensionless valve maneuver, with $\xi_r = \xi(T_c = (0.01{:}0.01{:}1)T, T_T = 2T,$ SNR = 10 dB, $d = 50$ m)$/\xi(T_c = 0.01T, T_T = 2T,$ SNR = 10 dB, $d = 50$ m), and T = fundamental water hammer period = 4 s.

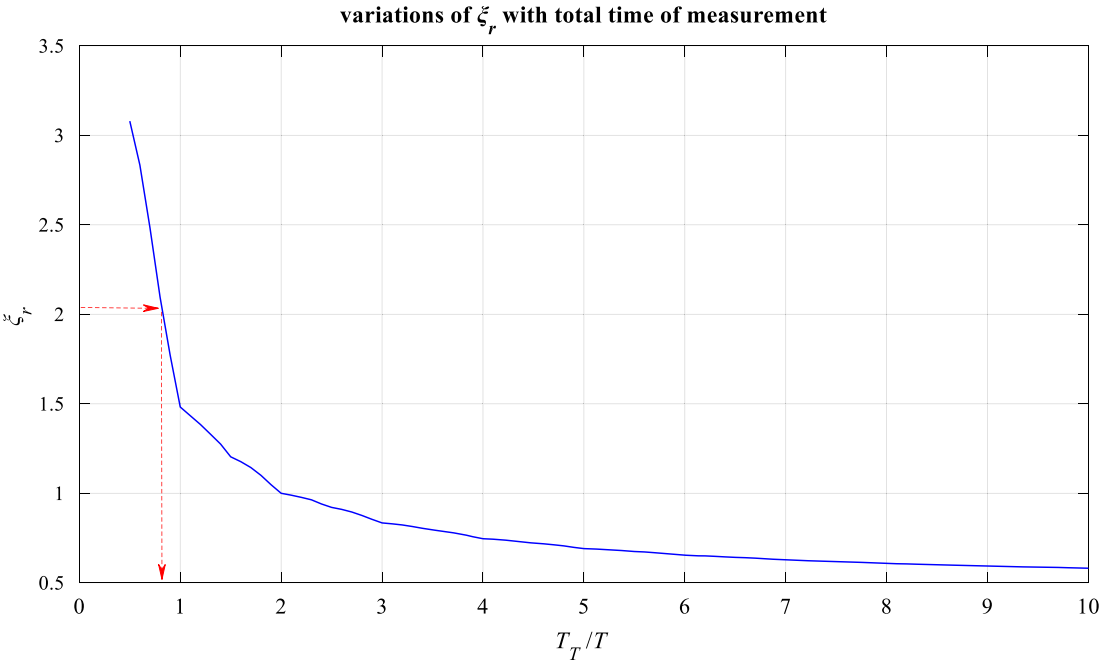

Fig. 9. Relative CR bound ξr as a function of dimensionless measurement time length, with $\xi_r = \xi(T_c = 0.01T, T_T = (0.5{:}0.2{:}10)T,$ SNR = 10 dB, $d = 50$ m)$/\xi(T_c = 0.01T, T_T = 2T,$ SNR = 10 dB, $d = 50$ m), [Eq. (10) defines ξ], and T = fundamental water hammer period = 4 s.

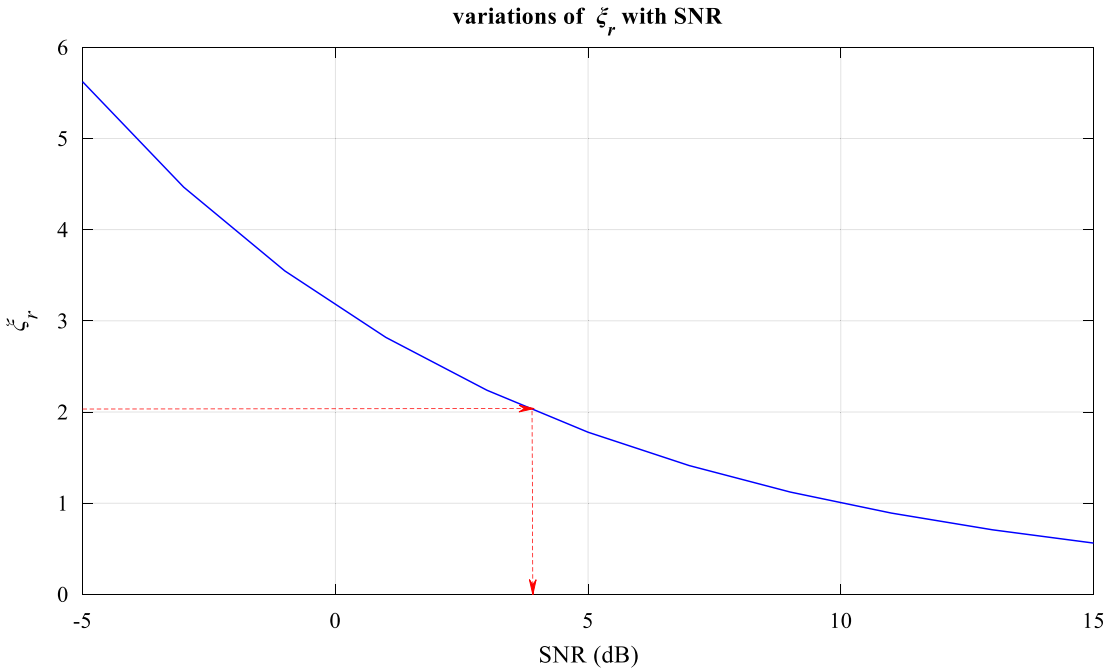

Fig. 10. Relative CR bound [Eq. (10) defines ξ] as a function of SNR, where $\xi(T_c = 0.01T, T_T = 2T, \text{SNR} = (-5{:}15)\text{dB}, d = 50\text{ m})/\xi(T_c = 0.01T, T_T = 2T, \text{SNR} = 10\text{ dB}, d = 50\text{ m})$, and T = water hammer period = 4 s.

than $2T$, the gain in certainty is relatively low. In other words, one does not benefit (gain in detection confidence) much by taking signals longer than $T_T = 2T$. For the desired target $\xi_r = 2$, CRLB shows that $T_T = 0.8T$ is appropriate for the transient experiment given $T_c = 0.01T$ and SNR = 10 dB. This also shows that when $T_T = 0.8T$ and $T_c = 0.01T$, the same certainty in detection as for the explained case in Fig. 8 is achieved.

Fig. 10 gives the variation of ξ_r with SNR for given $T_c = 0.01T$ and $T_T = 2T$. For a given target $\xi_r = 2$, CRLB shows that SNR = 4 dB can provide the required detection certainty. If the SNR increases (e.g., SNR = 10 dB), then the detection certainty rises, as shown in Figs. 10 and 6(a). Eventually, the transient experiment designed by using SNR = 4 dB (i.e., $\xi_r = 2$), $T_c = 0.01T$, and $T_T = 2T$ can still be acceptable by water authorities for localization because the position of leaks is usually the main concern of clients. For instance, Fig. 6(c) displays an experiment where ξ_r is higher than 2, but as discussed, the leak location can still be identified.

Ferrante et al. (2014) investigated different ways to increase the transient signal power and thus enhancing detectability. However, because they did not recognize noise interference in localization, no prescriptions for transient experiment design were deduced by their study. Nevertheless, the current research enables a systematic way to quantify the required values of transient test parameters for a successful leak identification with a specified resolution of size and location.

Probability of Successful Localization

This section uses the CRLB to estimate the highest probability of successful leakage localization. Assuming that the estimated leak sizes $\hat{\mathbf{A}}_\mathbf{e}$ follow Gaussian distribution with mean $\mathbf{A}_\mathbf{e}$ (actual value of leak sizes, i.e., they are unbiased estimators), then the probability density function (PDF) of $\hat{\mathbf{A}}_\mathbf{e}$ is obtained

$$p_L(\hat{\mathbf{A}}_\mathbf{e}) = \frac{1}{\sqrt{(2\pi)^{N_L}\det(\mathbf{\Sigma}_{\hat{\mathbf{A}}_\mathbf{e}})}}\exp\left(-\frac{1}{2}(\hat{\mathbf{A}}_\mathbf{e}-\mathbf{A}_\mathbf{e})^{\mathrm{T}}\mathbf{\Sigma}_{\hat{\mathbf{A}}_\mathbf{e}}^{-1}(\hat{\mathbf{A}}_\mathbf{e}-\mathbf{A}_\mathbf{e})\right)$$
$$= \frac{1}{\sqrt{(2\pi)^{N_L}\det(\mathbf{I}_{\hat{\mathbf{A}}_\mathbf{e}}^{-1})}}\exp\left(-\frac{1}{2}(\hat{\mathbf{A}}_\mathbf{e}-\mathbf{A}_\mathbf{e})^{\mathrm{T}}\mathbf{I}_{\hat{\mathbf{A}}_\mathbf{e}}(\hat{\mathbf{A}}_\mathbf{e}-\mathbf{A}_\mathbf{e})\right) \quad (11)$$

where $\mathbf{\Sigma}_{\hat{\mathbf{A}}_\mathbf{e}}$ and $\mathbf{I}_{\hat{\mathbf{A}}_\mathbf{e}}$ are, respectively, the covariance and Fisher information matrix of the leak sizes as derived in Eq. (8).

In a real-time leak detection exercise, localization is more important than sizing leaks. A criterion for successful localization based on the evaluated lower-bound error of leak sizes can be defined. Assume that a single leak is located at the kth node with size A_{ek}. The following criterion for successful localization of this leaky node can be defined:

$$A_{ek} - \sigma_{A_{ek}} > \sigma_{A_{ei}}, \quad i = \{1, 2, \ldots, N_L\}/\{k\} \quad (12)$$

which means that in the leak-detection runs of ITA, the estimated leak size at the actual location (indicated by index k) is maximum with a very high probability so that it can be identified in most cases. On the basis of the numerical manifestations in Figs. 1, 3, 6, and 7, one can assume that all nodes have similar standard deviations $\sigma_{A_{ek}} = \sigma_{A_{ei}}$; thus, Eq. (12) reduces to

$$\sigma_{A_{ei}} < \frac{A_{ek}}{2}, \quad i = \{1, 2, \ldots, N\} \quad (13)$$

In other words, the lower-bound error at all nodes should be smaller than $A_{ek}/2$. The criteria provided in Eq. (13) implies that the threshold of successful localization is $\sigma_{A_e} = A_{ek}/2$, which for the leak case under consideration is $\sigma_{A_e} = A_e/2 = 10\text{ mm}^2$, indicated by the dashed line in Fig. 5. The desired threshold σ_{A_e} along with the PDF defined by Eq. (11) can be exploited to estimate the highest probability of localization using the multivariable normal cumulative density function

$$p_L[(\hat{A}_{e1} - A_{e1} < \sigma_{A_e}) \cap (\hat{A}_{e2} - A_{e2} < \sigma_{A_e}) \cap \ldots \cap (A_{ek} - \hat{A}_{ek} < \sigma_{A_e}) \cap \ldots \cap (\hat{A}_{eN} - A_{eN} < \sigma_{A_e})]$$
$$= p_L[(\hat{A}_{e1} - A_{e1} < \sigma_{A_e}) \cap (\hat{A}_{e2} - A_{e2} < \sigma_{A_e}) \cap \ldots \cap (\hat{A}_{ek} - A_{ek} < \sigma_{A_e}) \cap \ldots \cap (\hat{A}_{eN} - A_{eN} < \sigma_{A_e})]$$
$$= p_L(\hat{\mathbf{A}}_\mathbf{e} - \mathbf{A}_\mathbf{e} < \sigma_{A_e}\mathbf{1}) = \int_{-\infty}^{A_{e1}+\sigma_{A_e}} \int_{-\infty}^{A_{e2}+\sigma_{A_e}} \ldots \int_{-\infty}^{A_{ek}+\sigma_{A_e}} \ldots \int_{-\infty}^{A_{eN}+\sigma_{A_e}} p_L(\hat{A}_{e1}, \hat{A}_{e2}, \ldots, \hat{A}_{eN}) d\hat{A}_{e1} d\hat{A}_{e2} \ldots d\hat{A}_{eN}, \sigma_{A_e} = 0.5A_e \quad (14)$$

where $\mathbf{1}$ is a column vector of ones with N_L elements. The second equality holds due to the symmetric property of the Gaussian distribution.

Fig. 11 shows the computed cumulative probabilities for different localization accuracy and various linear maneuver times. These results also confirm the findings in Fig. 5 regarding the fact that it is highly probable to find the leak in $(\hat{x}_L - a \cdot T_c, \hat{x}_L + a \cdot T_c)$. For localization in the region $(\hat{x}_L - d, \hat{x}_L + d)$ where $0.5a \cdot T_c < d < a \cdot T_c$, the probability reduces smoothly, and finally for $d < 0.5a \cdot T_c$, the successful probability has declined drastically. These curves reveal that for a given probability of successful localization, each valve maneuver time (probing bandwidth) can arrive at a certain accuracy in localization at best.

Conclusions

Noise in a measured signal can blur the desired reflections from leaks and reduce the amount of information that can be achieved from waves. It is therefore of great interest to quantify the maximum achievable information or lower bound of error in leak-size detection and localization. The main contributions of CRLB in terms of lower-bound error of leak-size estimates and experiment design have been addressed. For a hypothetical pipe system, the effect of valve-closure time and sample size of measurement on the computed lower bound error of leak-size estimates were investigated. The results revealed a sharp rise of standard deviation with increased time closure and conversely, a significant drop of error for higher time length of measurements. The behavior of the parameters demonstrated the importance of optimal design of time closure and measurement time duration corresponding to the desired accuracy.

The comparison of lower-bound error of size-detection with leak-size estimates allows for quantifying the success of localization. The assumption of lumping potential leaks at computational nodes indicated that only the error bound of leak sizes can be formulated. However, it was observed that the error of size detection rises with reduced distance between two consecutive leaks. The reason is the significant interaction between close leaks (closer than $a \cdot T_c/2$) or in another interpretation, the high correlation of the leak estimates when they are closer than half the minimum wavelength. The variation of leak-size error versus distance between two consecutive leaks enables one to predict the best possible resolution in localization for a given set of physical experimental parameters. The probability of successful localization within a specified zone (resolution) was further evaluated using the cumulative integration of the estimated PDF of leak sizes.

Using the CRLB computations, the efficient mesh size for ITA-based leak detection was proposed to be a constant factor of the length of the probing wavefronts $(a \cdot T_c)$. The factor is supposed to be a function of the shape of the wavefront, which is dictated by the valve closure pattern (Ferreira et al. 2018). For a linear closure, a factor around 0.5 is found, where a lower value raises the standard deviation and hence leads to inaccurate size estimates.

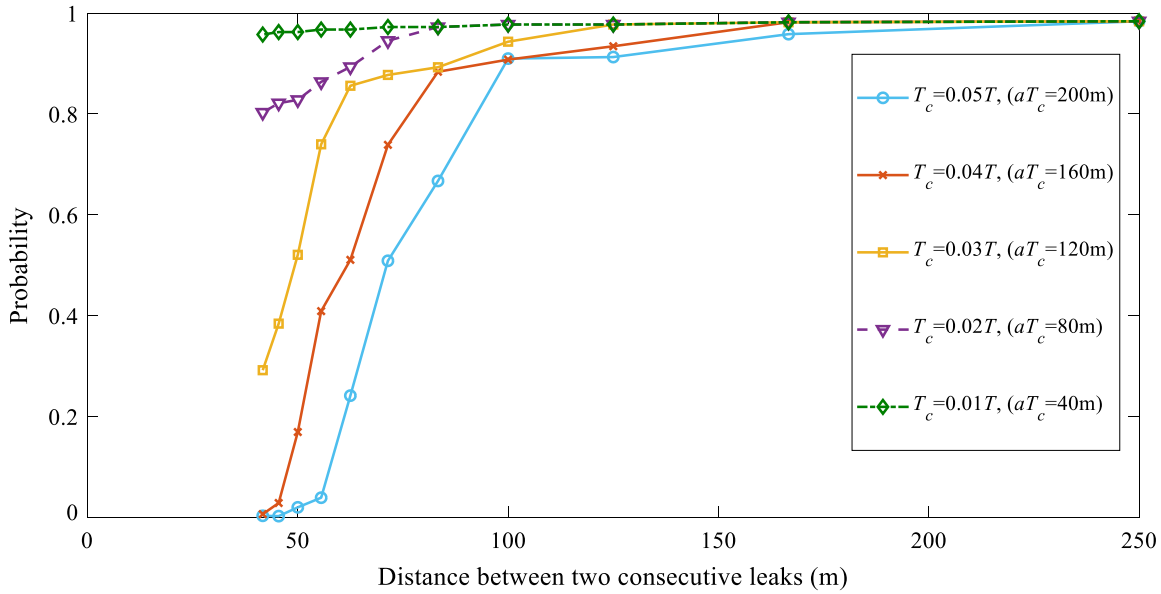

Fig. 11. Cumulative probability of successful localization versus different resolutions and valve maneuver, where $x_L = 500$ m, $A_e = 20$ mm^2, SNR = 10 dB, and $T_T = 2T$.

Appendix I. Second Derivative of the Log-Likelihood Function

The first derivative of the log-likelihood function in Eq. (4) is

$$\frac{\partial \mathrm{L}(\mathbf{A_e};\mathbf{h_m})}{\partial A_{ei}} = -\frac{1}{2\sigma^2}\frac{\partial \|(\mathbf{h_m}-\mathbf{h})\|^2}{\partial A_{ei}} = -\frac{1}{2\sigma^2}\frac{\partial(\mathbf{h_m^T h_m} - 2\mathbf{h_m^T h} + \mathbf{h^T h})}{\partial A_{ei}} = \frac{1}{\sigma^2}\frac{\partial \mathbf{h}^{\mathrm{T}}}{\partial A_{ei}}(\mathbf{h_m}-\mathbf{h}) \tag{15}$$

Second derivative yields

$$\frac{\partial^2 \mathrm{L}(\mathbf{A_e};\mathbf{h_m})}{\partial A_{ei}\partial A_{ej}} = \frac{1}{\sigma^2}\frac{\partial}{\partial A_{ej}}\left[\frac{\partial \mathbf{h}^{\mathrm{T}}}{\partial A_{ei}}(\mathbf{h_m}-\mathbf{h})\right] = \frac{1}{\sigma^2}\left[\frac{\partial^2 \mathbf{h}^{\mathrm{T}}}{\partial A_{ei}\partial A_{ej}}(\mathbf{h_m}-\mathbf{h}) - \frac{\partial \mathbf{h}^{\mathrm{T}}}{\partial A_{ei}}\frac{\partial \mathbf{h}}{\partial A_{ej}}\right] \tag{16}$$

Appendix II. Direct Differentiation Method

The following algorithm can be utilized to compute the sensitivities of the state variables at each point and time step with respect to the leak-size parameters. At the steady state, the head and flow rate at reservoir node (node number $k = 1$) are known. Therefore, for the reservoir node

$$\frac{\partial h_1}{\partial A_{ei}} = 0, \quad \frac{\partial Q_{1+}}{\partial A_{ei}} = 0 \tag{17}$$

where flow rate before and after the leak are indicated by minus and plus subscripts, respectively. For each interior node $1 < k < N_n$, three relations including continuity and orifice relation at each node and Darcy-Weisbach head loss between leaks hold (Fig. 12), which taking their derivative with respect to leak sizes yields

$$\frac{\partial Q_{k,-}}{\partial A_{ei}} = \frac{\partial Q_{k-1,+}}{\partial A_{ei}},$$
$$\frac{\partial h_k}{\partial A_{ei}} = \frac{\partial h_{k-1}}{\partial A_{ei}} - \frac{f\Delta x Q_{k-1,+}}{gDA^2}\frac{\partial Q_{k-1,+}}{\partial A_{ei}}, \quad k = 2, 3, \ldots, N_n \tag{18}$$

$$\frac{\partial Q_{k,+}}{\partial A_{ei}} = \frac{\partial Q_{k,-}}{\partial A_{ei}} - \sqrt{2g(h_k - h_o)}\left(\frac{\partial A_{ek}}{\partial A_{ei}} + \frac{A_{ek}}{2(h_k - h_o)}\frac{\partial h_k}{\partial A_{ei}}\right) \tag{19}$$

where g = gravitational acceleration; and h_o = pressure head outside the pipe (to compute head difference inside and outside the pipe at the leak). If $k = i$, then $\partial A_{ek}/\partial A_{ei} = 1$; otherwise, it is zero. These computations should be implemented sequentially from the reservoir point to the downstream valve or vice versa (if the head and flow rate at the valve, rather than reservoir, are given).

At the transient state, the goal is to compute the derivatives at the next time step knowing those at the current step. The algebraic (finite difference) form of the characteristics equations in the presence of leak at each node are used for this aim

$$\mathrm{C}^+: Q_{k-} = -C_{ap}h_k + C_p \tag{20}$$

$$\mathrm{C}^-: Q_{k+} = C_{an}h_k + C_n \tag{21}$$

where subscripts p and n = positive and negative characteristic lines; and coefficients C_{ap}, C_p, C_{an}, and C_n = general functions of head and flow rate at the current time step and flow and pipe parameters (Chaudhry 2014; Wylie and Streeter 1993; Soares et al. 2008; Keramat et al. 2012). Their derivatives with respect to each leak area $\partial C_n/\partial A_{ei}$, $\partial C_p/\partial A_{ei}$, $\partial C_{ap}/\partial A_{ei}$, and $\partial C_{an}/\partial A_{ei}$ are conveniently determined because the derivative of the state variables (head and discharge) at the current step is known; they were already found in Eqs. (17)–(19) for the first time step (steady state).

Eqs. (20) and (21) along with the orifice relation (Brunone 1999)

$$Q_{k-} - Q_{k+} = A_{ek}\sqrt{2g(h_k - h_o)} \tag{22}$$

are simultaneously solved for the three unknowns Q_{k-}, Q_{k+}, and h_k at each computational section. The solution yields the following explicit expression for h_k:

$$h_k = -\frac{A_{ek}\alpha^{0.5} - gA_{ek}^2 + C_nC_{an} + C_nC_{ap} - C_pC_{an} - C_pC_{ap}}{(C_{an} + C_{ap})^2} \quad \text{with}$$
$$\alpha = -g(2C_{an}^2h_o - gA_{ek}^2 + 2C_{ap}^2h_o + 2C_nC_{an} + 2C_nC_{ap} - 2C_pC_{an} - 2C_pC_{ap} + 4C_{an}C_{ap}h_o) \tag{23}$$

Finally, the chain rule allows for the sensitivity computation at the next time step

$$\frac{dh_k}{dA_{ei}} = \frac{\partial h_k}{\partial C_n}\frac{\partial C_n}{\partial A_{ei}} + \frac{\partial h_k}{\partial C_p}\frac{\partial C_p}{\partial A_{ei}} + \frac{\partial h_k}{\partial C_{ap}}\frac{\partial C_{ap}}{\partial A_{ei}} + \frac{\partial h_k}{\partial C_{an}}\frac{\partial C_{an}}{\partial A_{ei}} + \frac{\partial h_k}{\partial A_{ei}} \tag{24}$$

Eqs. (20) and (21) are also symbolically differentiated to calculate derivatives of Q_{k+} and Q_{k-} with respect to the leak variables.

Appendix III. Correlation between Leak Estimates

The correlation between ith and jth leak candidates is numerically found using the evaluated lower bound of the covariance matrix in Eq. (8), as follows:

$$r_{A_{ei},A_{ej}} = \frac{\mathrm{cov}(A_{ei}, A_{ej})}{\sigma_{A_{ei}}\sigma_{A_{ej}}}, \quad i, j = 1, 2, \ldots, N_L \tag{25}$$

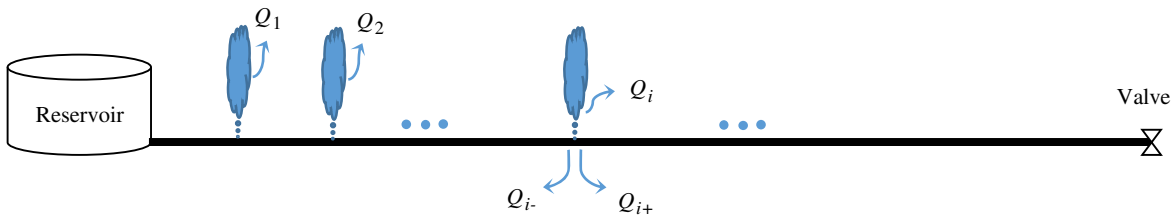

Fig. 12. Schematic of a reservoir-multileak pipe valve system for the computation of sensitivities. Q_1, Q_2, and Q_i stand for discharge of leaks and Q_{i-} and Q_{i+} represent discharge before and after each leak, respectively.

J. Hydraul. Eng., 2019, 145(6): 04019018

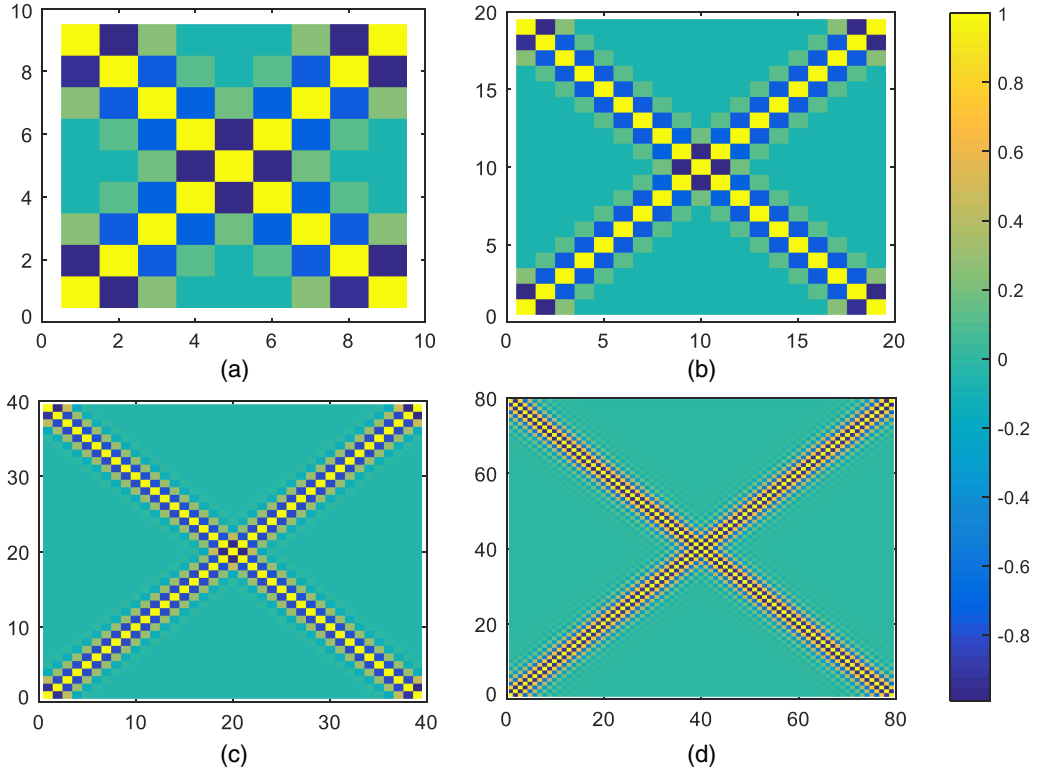

Fig. 13. Scaled shading representation of computed correlation matrices for runs with different numbers of leak candidates. Numbers on x- and y-axes indicate the element indices of each matrix.

where $\sigma_{A_{ei}}$ and $\sigma_{A_{ej}}$ = standard deviations for ith and jth leak so the diagonal elements of the correlation matrix are equal to 1. The values of this matrix for different number of potential leaks are indicated by shading in Fig. 13. Generally, these matrices show that there is a negative correlation between two consecutive leaks and the amount of this negative correlation increases when the leaks get closer. More precisely, it means that any change in the size of one leak can be compensated by a negative change, which corresponds to negative leak size (inflow) at the next point. In addition, for quite close leaks [Fig. 13(d)], there is a sequence of negative and positive correlations between serial leaks, which intuitively means that the signature of one leak on the pressure signal can be reconstructed by sequential inflows and outflows (leaks) at successive neighboring nodes. As a result of considerable negative (positive) correlation between each leak and its neighboring one observed in the second (third) off-diagonal elements from the main diagonal, one can anticipate that higher standard deviations for leak sizes are likely for the same set of data.

Acknowledgments

This work has been supported by research grants from the Research Grant Council of the Hong Kong SAR, China (Project Nos. T21-602/15R and 16208618). The authors would like to thank Duncan McInnis, Fedi Zouari, Asgar Ahadpour, Man Yue Lam, and Jingrong Lin for their helpful comments and discussions.

Notation

The following symbols are used in this paper:

$\mathbf{A_e}$ = effective leak-area of all leak candidates;
$\hat{\mathbf{A}}_\mathbf{e}$ = estimated effective leak area of all leak candidates;
A_{ei} = effective leak area at node i;
$\hat{A}_{ei}$ = estimated effective leak area at node i;
a = wave speed;
d = distance between potential leaks (resolution of leak localization);
$\mathbf{h} = \mathbb{E}(\mathbf{h_m})$ = expectation of measured pressure signal = computed pressure head;
$\mathbf{h_m}$ = measured pressure head;
$\mathbf{I}$ = Fisher information matrix;
L = pipe length;
L = likelihood function;
M = number of measurement time points;
N_L = number of leak candidates;
p_L = probability density function of estimated leaks;
T = water hammer period;
T_T = total time of measurement;
T_c = manoeuvre time of valve;
Δx = mesh (grid) size of MOC numerical solution;
$\lambda = aT_c$ = length of injected wavefront = wavelength;
ξ = average Cramer-Rao bound of leak candidates [Eq. (10)]; and
σ = noise standard deviation = standard deviation of measured pressures.

References

Ahmadi, A., and A. Keramat. 2010. "Investigation of fluid-structure interaction with various types of junction coupling." *J. Fluids Struct.* 26 (7–8): 1123–1141. https://doi.org/10.1016/j.jfluidstructs.2010.08.002.

Bolliger, C. S., C. Boesch, and R. Kreis. 2013. "On the use of Cramér-Rao minimum variance bounds for the design of magnetic resonance

spectroscopy experiments." *Neuroimage* 83: 1031–1040. https://doi.org/10.1016/j.neuroimage.2013.07.062.

Brunone, B. 1999. "Transient test-based technique for leak detection in outfall pipes." *J. Water Resour. Plann. Manage.* 125 (5): 302–306. https://doi.org/10.1061/(ASCE)0733-9496(1999)125:5(302).

Brunone, B., and M. Ferrante. 2001. "Detecting leaks in pressurized pipes by means of transients." *J. Hydraul. Res.* 39 (5): 539–547. https://doi.org/10.1080/00221686.2001.9628278.

Chaudhry, M. H. 2014. *Applied hydraulic transients*. 3rd ed. New York: Springer.

Colombo, A. F., P. Lee, and B. W. Karney. 2009. "A selective literature review of transient-based leak detection methods." *J. Hydro-Environ. Res.* 2 (4): 212–227. https://doi.org/10.1016/j.jher.2009.02.003.

Conte, J. P., P. K. Vijalapura, and M. Meghella. 2003. "Consistent finite-element response sensitivity analysis." *J. Eng. Mech.* 129 (12): 1380–1393. https://doi.org/10.1061/(ASCE)0733-9399(2003)129:12(1380).

Covas, D., I. Stoianov, J. Mano, H. Ramos, N. Graham, and C. Maksimovic. 2005. "The dynamic effect of pipe-wall viscoelasticity in hydraulic transients. Part II-Model development, calibration and verification." *J. Hydraul. Res.* 43 (1): 56–70. https://doi.org/10.1080/00221680509500111.

Diong, M. L., A. Roueff, L. Philippe, and A. Litman. 2015. "Precision analysis based on Cramer-Rao bound for 2D acoustics and electromagnetic inverse scattering." *Inverse Prob.* 31 (7): 075003. https://doi.org/10.1088/0266-5611/31/7/075003.

Duan, H. 2016. "Sensitivity analysis of a transient-based frequency domain method for extended blockage detection in water pipeline systems." *J. Water Resour. Plann. Manage.* 142 (4): 04015073. https://doi.org/10.1061/(ASCE)WR.1943-5452.0000625.

Ferrante, M., B. Brunone, and S. Meniconi. 2007. "Wavelets for the analysis of transient pressure signals for leak detection." *J. Hydraul. Eng.* 133 (11): 1274–1282. https://doi.org/10.1061/(ASCE)0733-9429(2007)133:11(1274).

Ferrante, M., B. Brunone, and S. Meniconi. 2010. "Leak-edge detection." *J. Hydraul. Res.* 47 (2): 233–241. https://doi.org/10.3826/jhr.2009.3220.

Ferrante, M., B. Brunone, and S. Meniconi. 2014. "Leak size, detectability and test conditions in pressurized pipe systems." *Water Resour. Manage.* 28 (13): 4583–4598. https://doi.org/10.1007/s11269-014-0752-6.

Ferrante, M., C. Capponi, R. Collins, J. Edwards, B. Brunone, and S. Meniconi. 2016. "Numerical transient analysis of random leakage in time and frequency domains." *Civ. Eng. Environ. Syst.* 33 (1): 70–84. https://doi.org/10.1080/10286608.2016.1138941.

Ferreira, J. P. B. C. C., N. M. C. Martins, and D. I. C. Covas. 2018. "Ball valve behavior under steady and unsteady conditions." *J. Hydraul. Eng.* 144 (4): 04018005. https://doi.org/10.1061/(ASCE)HY.1943-7900.0001434.

Garthwaite, P., I. Jolliffe, and B. Jones. 2002. *Statistical inference*. 2nd ed. London: Oxford Science Publications.

Greenspan, H. 2008. "Super-resolution in medical imaging." *Comput. J.* 52 (1): 43–63. https://doi.org/10.1093/comjnl/bxm075.

Haghighi, A., H. M. Ramos. 2012. "Detection of leakage freshwater and friction factor calibration in drinking networks using central force optimization." *Water Resour. Manage.* 26 (8): 2347–2363. https://doi.org/10.1007/s11269-012-0020-6.

Jung, B. S., and B. W. Karney. 2008. "Systematic exploration of pipeline network calibration using transients." *J. Hydraul. Res.* 46: 129–137. https://doi.org/10.1080/00221686.2008.9521947.

Kapelan, Z. S., D. A. Savic, and G. A. Walters. 2003. "A hybrid inverse transient model for leakage detection and roughness calibration in pipe networks." *J. Hydraul. Res.* 41 (5): 481–492. https://doi.org/10.1080/00221680309499993.

Kay, S. M. 1993. *Fundamentals of statistical signal processing. Vol. 1 of estimation theory.* Englewood Cliffs, NJ: Prentice-Hall.

Keramat, A., A. Gaffarian Kolahi, and A. Ahmadi. 2013. "Waterhammer modelling of viscoelastic pipes with a time-dependent Poisson's ratio." *J. Fluids Struct.* 43: 164–178. https://doi.org/10.1016/j.jfluidstructs.2013.08.013.

Keramat, A., and A. S. Tijsseling. 2012. "Waterhammer with column separation, fluid-structure interaction and unsteady friction in a viscoelastic pipe." In *Proc., 11th Int. Conf. on Pressure Surges*, edited by S. Anderson, 443–460. Bedford, UK: BHR Group.

Keramat, A., A. S. Tijsseling, Q. Hou, and A. Ahmadi. 2012. "Fluid-structure interaction with pipe-wall viscoelasticity during water hammer." *J. Fluids Struct.* 28: 434–455. https://doi.org/10.1016/j.jfluidstructs.2011.11.001.

Kleiber, M., H. Antunez, T. D. Hien, and P. Kowalczyk. 1997. *Parameter sensitivity in nonlinear mechanics: Theory and finite element computations*. Chichester, UK: Wiley.

Lee, P. J., H. F. Duan, M. Ghidaoui, and B. Karney. 2013. "Frequency domain analysis of pipe fluid transient behavior." *J. Hydraul. Res.* 51 (6): 609–622. https://doi.org/10.1080/00221686.2013.814597.

Lee, P. J., H. F. Duan, J. Tuck, and M. Ghidaoui. 2015. "Numerical and experimental study on the effect of signal bandwidth on pipe assessment using fluid transients." *J. Hydraul. Eng.* 141 (2): 04014074. https://doi.org/10.1061/(ASCE)HY.1943-7900.0000961.

Liggett, J. A., and L. C. Chen. 1994. "Inverse transient analysis in pipe networks." *J. Hydraul. Eng.* 120 (8): 934–955. https://doi.org/10.1061/(ASCE)0733-9429(1994)120:8(934).

Louati, M., M. Meniconi, M. S. Ghidaoui, and B. Brunone. 2017. "Experimental study of the eigenfrequency shift mechanism in blocked pipe system." *J. Hydraul. Eng.* 143 (10): 04017044. https://doi.org/10.1061/(ASCE)HY.1943-7900.0001347.

Majd, A., A. Ahmadi, and A. Keramat. 2016. "Investigation of non-Newtonian fluid effects during transient flows in a pipeline." *Strojniški vestnik/J. Mech. Eng.* 62 (2): 105–115. https://doi.org/10.5545/sv-jme.2015.2787.

McCutchen, C. W. 1967. "Super-resolution in microscopy and the Abbe resolution limit." *J. Opt. Soc. Am.* 57 (10): 1190. https://doi.org/10.1364/JOSA.57.001190.

Meniconi, S., B. Brunone, M. Ferrante, and C. Massari. 2014. "Energy dissipation and pressure decay during transients in viscoelastic pipes with an in-line valve." *J. Fluids Struct.* 45: 235–249. https://doi.org/10.1016/j.jfluidstructs.2013.12.013.

Meniconi, S., B. Brunone, M. Frisinghelli, E. Mazzetti, M. Larentis, and C. Costisella. 2017. "Safe transients for pipe survey in a real transmission main by means of a portable device: The case study of the Trento (I) supply system." *Procedia Eng.* 186: 228–235. https://doi.org/10.1016/j.proeng.2017.03.232.

Nash, G. A., and B. W. Karney. 1999. "Efficient inverse transient analysis in series pipe systems." *J. Hydraul. Eng.* 125 (7): 761–764. https://doi.org/10.1061/(ASCE)0733-9429(1999)125:7(761).

Nehorai, A., and M. Hawkes. 2000. "Performance bounds for estimating vector systems." *IEEE Trans. Signal Process.* 48 (6): 1737–1749. https://doi.org/10.1109/78.845931.

Oppenheim, A. V., A. S. Willsky, and I. T. Young. 1983. *Signals and systems*. 15th ed. Englewood Cliffs, NJ: Prentice-Hall.

Press, W. H., S. A. Teukolsky, W. T. Vetterling, and B. P. Flannery. 1992. *Numerical recipes: The art of scientific computing*. Cambridge, UK: Cambridge University Press.

Puschmann, K. G., and F. Kneer. 2005. "On super-resolution in astronomical imaging." *Astron. Astrophys.* 436 (1): 373–378. https://doi.org/10.1051/0004-6361:20042320.

Robinson, D., and P. Milanfar. 2006. "Statistical performance analysis of super-resolution." *IEEE Trans. Image Process.* 15 (6): 1413–1428. https://doi.org/10.1109/TIP.2006.871079.

Sattar, A. M., and M. El-Beltagy. 2017. "Stochastic solution to the water hammer equations using polynomial chaos expansion with random boundary and initial conditions." *J. Hydraul. Eng.* 143 (2): 04016078. https://doi.org/10.1061/(ASCE)HY.1943-7900.0001227.

Shannon, C. E. 1949. "Communication in the presence of noise." *Proc. IRE* 37 (1): 10–21. https://doi.org/10.1109/JRPROC.1949.232969.

Soares, A. K., D. I. C. Covas, and L. F. Reis. 2008. "Analysis of PVC pipe-wall viscoelasticity during water hammer." *J. Hydraul. Eng.* 134 (9): 1389–1394. https://doi.org/10.1061/(ASCE)0733-9429(2008)134:9(1389).

van Trees, H. L., and K. Bell. 2013. *Detection, estimation, and modulation theory: I. Detection, estimation, and filtering theory.* 2nd ed. New York: Wiley.

Vaseghi, S. 2008. *Advanced digital signal processing and noise reduction*. 4th ed. Chichester, UK: Wiley.

Vitkovsky, J., M. Lambert, A. Simpson, and J. Liggett. 2007. "Experimental observation and analysis of inverse transients for pipeline leak detection." *J. Water Resour. Plann. Manage.* 136 (6): 519–530. https://doi.org/10.1061/(ASCE)0733-9496(2007)133:6(519).

Vitkovsky, J. P., J. Liggett, A. R. Simpson, and M. F. Lambert. 2003. "Optimal measurement site locations for inverse transient analysis in pipe networks." *J. Water Resour. Plann. Manage.* 129 (6): 480–492. https://doi.org/10.1061/(ASCE)0733-9496(2003)129:6(480).

Vítkovský, J. P., A. R. Simpson, and M. F. Lambert. 2000. "Leak detection and calibration using transients and genetic algorithms." *J. Water Resour. Plann. Manage.* 126 (4): 262–265. https://doi.org/10.1061/(ASCE)0733-9496(2000)126:4(262).

Wang, X., and M. S. Ghidaoui. 2018a. "Identification of multiple leaks in pipeline: Linearized model, maximum likelihood, and super-resolution localization." *Mech. Syst. Signal Process.* 107: 529–548. https://doi.org/10.1016/j.ymssp.2018.01.042.

Wang, X., and M. S. Ghidaoui. 2018b. "Pipeline leak detection using the matched-field processing method." *J. Hydraul. Eng.* 144 (6): 04018030. https://doi.org/10.1061/(ASCE)HY.1943-7900.0001476.

Wang, X., D. P. Palomar, L. Zhao, M. S. Ghidaoui, and R. D. Murch. 2019. "Spectral-based methods for pipeline leak detection." *J. Hydraul. Eng.* 145 (3): 04018089. https://doi.org/10.1061/(ASCE)HY.1943-7900.0001572.

Wylie, E. B., and V. L. Streeter. 1993. *Fluid transients in systems*. Englewood Cliffs, NJ: Prentice-Hall.

Zhao, M., M. S. Ghidaoui, M. Louati, and H. F. Duan. 2018. "Numerical study of the blockage length effect on the transient wave in pipe flows." *J. Hydraul. Res.* 56 (2): 245–255. https://doi.org/10.1080/00221686.2017.1394374.

Zhao, W., J. Yu, A. Zhang, and Y. Li. 2014. "Optimal sensors deployment for tracking level curve based on posterior Cramér-Rao lower bound in scalar field." In Vol. 8917 of *Intelligent robotics and applications: Lecture notes in computer science (including subseries lecture notes in artificial intelligence and lecture notes in bioinformatics)*, 129–141. Cham, Switzerland: Springer.